Astron. Astrophys. 316, 441–448 (1996)

ASTRONOMY
AND
ASTROPHYSICS

Coronal radio sounding with Ulysses: solar wind electron density near 0.1 AU during the 1995 conjunction

M.K. Bird[1], **M. Pätzold**[2], **P. Edenhofer**[3], **S.W. Asmar**[4], **and T.P. McElrath**[4]

[1] Radioastronomisches Institut, Universität Bonn, Auf dem Hügel 71, D-53121 Bonn, Germany
[2] Institut für Geophysik und Meteorologie, Universität zu Köln, Albertus-Magnus-Platz, D-50923 Köln, Germany
[3] Institut für HF-Technik, Universität Bochum, D-44780 Bochum, Germany
[4] Jet Propulsion Laboratory, California Institute of Technology, Pasadena, CA 91109, USA

Received 18 March 1996 / Accepted 15 May 1996

Abstract. Dual-frequency ranging measurements were recorded for a three-week interval during the 1995 solar conjunction of the Ulysses spacecraft. The unusual occultation geometry resulting from the high inclination Ulysses orbit enabled coronal radio sounding from the solar South Pole to the heliographic equator at solar ray path offsets near 0.1 AU. The electron column density along the line-of-sight between Ulysses and Earth, derived from the differential time delays of ranging signals transmitted simultaneously on S-band and X-band carriers, clearly show the signatures of the polar coronal hole and a streamer belt at low latitudes. The observations are utilized in this work to test models for the heliographic latitude dependence of the electron density in the inner heliosphere. Traditional models for solar activity minimum, whereby the density decreases rather slowly from equator to pole, were found to fare rather poorly in representing the measurements. In contrast, a model based on Ulysses *in situ* solar wind measurements, when combined with ancillary observations to derive the location of the heliospheric current sheet, was found to provide satisfactory agreement with the radio sounding data.

Key words: occultations – Sun: corona

1. Introduction

The Ulysses Solar Corona Experiment (SCE), a dual-frequency downlink radio-sounding investigation, was performed during the spacecraft's fourth superior solar conjunction (C_4) in February–March 1995. The conjunction geometry was significantly different from those associated with spacecraft in or near the ecliptic plane. The combined motion of Ulysses (32.6 km s^{-1}, essentially perpendicular to the ecliptic) and Earth (30.0 km s^{-1} in the ecliptic), resulted in a unique opportunity to record measurements of electron column density N_T at all latitudes in the southwest quadrant of the solar corona from South Pole to heliographic equator at an approximately constant solar offset distance (solar proximate point along the radio ray path) near 0.1 AU. Conventional in-ecliptic radio-sounding opportunities, such as the Ulysses conjunction C_1 that occurred during the interplanetary cruise prior to the swing-by at Jupiter (Bird et al. 1994), are better suited for global-scale studies of the radial dependence of the electron density in the inner heliosphere. SCE measurements were not possible during the geometically less favorable conjunctions C_2 (September 1992) and C_3 (September 1993) because of spacecraft operational constraints on S-band transmission.

Although the primary dependence of the coronal density is radial, there is no doubt that latitudinal and longitudinal variations have left their imprint on measurements of N_T recorded during previous solar occultation experiments with spacecraft near the ecliptic plane. The asymmetric radial profiles derived for east and west limb observations during the 1985 Voyager experiment (Anderson et al. 1987), for example, were probably a result of different solar wind source regions rotating into and out of the radio ray paths over the duration of the occultation (Woo 1996). There have been other solar conjunction observations with significant latitudinal coverage, such as that of the Viking spacecraft in 1976 (Tyler et al. 1977; Muhleman & Anderson 1981), but the rapidly changing solar offset distance, and associated rapid variation in the measured electron content, renders these data sets less appropriate for analysis of coronal latitudinal structure. This problem is less severe for interplanetary scintillation (IPS) measurements, because there are many more natural radio sources at higher elongation to the ecliptic (e.g. Kojima & Kakinuma 1987; Rickett & Coles 1991; Coles et al. 1995; Manoharan 1993).

Dual-frequency ranging and Doppler measurements of the coherent downlinks at S-band (λ = 13.1 cm) and X-band (λ = 3.6 cm) were recorded around the clock during C_4 using the 34-m standard antennas of the NASA Deep Space Network (DSN) at sites in California (Deep Space Station DSS 12), Australia

Send offprint requests to: M.K. Bird

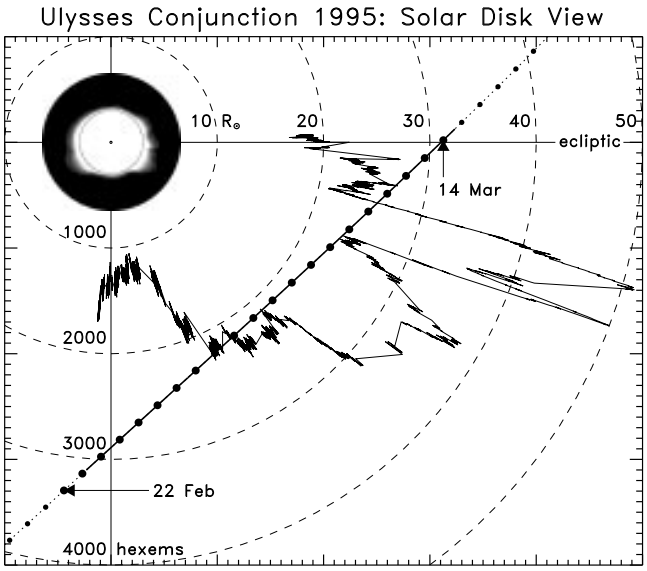

Fig. 1. Ulysses 1995 solar occultation geometry as viewed in the plane of the sky from Earth. The experiment was conducted during operation of the spacecraft's S-band downlink from 22 February to 14 March. Concentric circles denote solar offset distances at intervals of 10 $R_\odot$. Larger dots along the trajectory denote the spacecraft's position at 0 UT for each day. The time interval of actual measurements is indicated by the thick solid line along the trajectory. Measurements of the electron column density (jagged line) are displayed as a polar plot with the radial scale given along the south polar axis in units of hexems (10^{16} electrons m^{-2}). Centered on the position of the Sun is a grayscale image of the corona (3× natural size), taken at the Mauna Loa Solar Observatory with the Mark III coronagraph on 8 March 1995 (courtesy High Altitude Observatory).

(DSS 42) and Spain (DSS 61). A first analysis of the Doppler recordings is presented in an accompanying paper (Pätzold et al. 1996). Initial SCE results from C_4 comparing the ranging data with coronal source surface maps were presented by Pätzold et al. (1995). A description of the scientific goals and technical capabilities of the Ulysses coronal-sounding experiment may be found in Bird et al. (1992). The emphasis of this work is a comparison of the dual-frequency ranging measurements with calculations using various models of the heliolatitude dependence of the coronal electron density.

2. Experimental description and observations

2.1. Conjunction geometry

Figure 1 is an Earth-based view of C_4, showing Ulysses' virtual position in the plane of the sky with respect to the solar disk (solar ecliptic coordinates). A grayscale image of the corona from 8 March 1995, magnified by a factor of three, is placed at the position of the Sun. Also shown in Fig. 1 is a pictorial summary of the observations: a polar plot of the electron content measured at each solar position angle along the trajectory according to the scale given along the south polar axis (details in next subsection).

The spacecraft attained C_4 (minimum Sun-Earth-Probe angle: 5.8° ⇒ solar offset distance R = 21.4 $R_\odot$) on 4 March 1995 (day-of-year DOY 63), just prior to its perihelion and transit through the ecliptic plane. SCE observations began with activation of the S-band transmitter on 22 February 1995 (DOY 53) at a solar offset $R \sim 32$ $R_\odot$ below the solar South Pole. The S-band downlink had not been operated since the Jupiter encounter, when radio-sounding measurements were taken during the occultation of the Io plasma torus (Bird et al. 1993). The S-band was switched off again on 14 March 1995 (DOY 73), just after the spacecraft crossed over into the northern ecliptic hemisphere.

2.2. Dual-frequency ranging measurements

The group velocity of a modulated S-band signal propagating through an ionized medium is lower than that at X-band. This causes a slight delay in the arrival times for the various components of a ranging code transmitted simultaneously at these two carrier frequencies. This time delay is directly proportional to the columnar electron density N_T ("total electron content") along the downlink ray path (Bird & Edenhofer 1990). The ranging measurements must be corrected for a number of frequency-dependent contributions to signal delay inherent to the ground station and the spacecraft. These are described in detail in an earlier report (Bird et al. 1994).

For the Ulysses radio subsystem with coherent downlink frequencies (f_X/f_S = 11/3), the differential time delay is given by:

$$\Delta\tau = \frac{40.31}{c}\left[f_S^{-2} - f_X^{-2}\right] N_T \quad \simeq \quad 0.237 N_T \tag{1}$$

where c is the speed of light and f_S = 2.293 GHz and f_X = 8.408 GHz are the S- and X-band frequencies, respectively. The expression on the right in Eq. (1) holds for the differential delay time $\Delta\tau$ in nanoseconds and the total electron content N_T in "hexems", where the hexem is defined as 10^{16} electrons m^{-2}.

The total electron content is the integral of the electron density along the ray path from Ulysses to Earth:

$$N_T(R,\Theta,\Phi) = \int_{\text{Ulysses}}^{\text{Earth}} N(\mathbf{r})\, ds \tag{2}$$

where (R,Θ,Φ) are the heliographic polar coordinates of the solar offset point, and $N(\mathbf{r})$ is the electron density at an arbitrary position $\mathbf{r}$ on the ray path ds. There is a small contribution to N_T from the terrestrial ionosphere that typically reaches a diurnal maximum of ∼50 hexems. The ionospheric fraction of the total electron content probably never exceeds 5% during C_4 and is thus neglected for this work.

All measurements of coronal electron content N_T from Eq. (1) are plotted in polar coordinates for each solar position angle in Fig. 1. Because C_4 occurred when the Earth happened to be close to its maximum southern heliographic latitude (i.e., solar rotation axis tilted almost directly away from Earth), the solar ecliptic position angle in Fig. 1 is very close to the heliographic latitude Θ of the solar offset point. The relatively low

electron content observed during the first few days of the experiment, as expected for the solar minimum conditions in early 1995, is a consequence of the large-scale coronal hole over the Sun's South Pole. A significant enhancement in N_T was observed at lower latitudes, particularly starting on 8 March 1995 (DOY 67), when the solar proximate point was located at heliolatitudes from 16–21°S. This is now known to be the signature of the heliospheric current sheet (HCS), the extension of the coronal streamer belt into interplanetary space, which rotated into the Ulysses/Earth line-of-sight on these days. The streamer belt is clearly seen in the overlaid image of the corona in Fig. 1 from the Mauna Loa Solar Observatory (courtesy High Altitude Observatory). The mean value and standard deviation of electron content measured during each of the 42 DSN tracking passes during C_4, together with the applicable coordinates of the solar offset point (R,Θ), are listed in Table 1.

Table 1. Ulysses mean range measurements during C_4

DSS	range points	1995 DOY [UT]	N_T (σ_{N_T}) [hexem]	R [$R_\odot$]	Θ [deg]
42	36	54.28777	1561.6 (80.0)	31.3	-84.3
61	36	54.60068	1383.6 (68.3)	30.8	-85.4
42	89	55.18465	1379.4 (43.9)	29.8	-87.2
61	34	55.52994	1278.3 (68.8)	29.2	-88.1
42	112	56.15414	1331.4 (56.1)	28.2	-88.8
61	35	56.44170	1237.3 (35.8)	27.7	-87.7
12	20	56.81228	1231.9 (50.6)	27.2	-86.3
42	116	57.12179	1258.9 (42.4)	26.7	-85.1
61	42	57.45745	1164.0 (47.5)	26.2	-83.5
12	19	57.81604	1167.9 (49.8)	25.7	-81.9
42	115	58.11947	1256.2 (48.5)	25.3	-80.5
61	38	58.45110	1214.2 (58.1)	24.9	-78.8
61	88	59.53860	1408.6 (77.9)	23.7	-73.1
42	100	60.12145	1852.9 (86.7)	23.1	-69.9
61	29	60.44640	1905.5 (70.5)	22.8	-68.0
42	115	61.12016	2168.4 (49.2)	22.2	-63.9
12	24	61.80421	2109.4 (41.9)	21.9	-59.6
42	117	62.11612	2280.4 (57.1)	21.8	-57.6
61	39	62.43051	2301.3 (36.3)	21.7	-55.6
42	112	63.11233	2341.9 (41.9)	21.5	-51.0
61	89	63.54079	2251.3 (71.9)	21.4	-48.2
42	119	64.11104	2690.0 (234.5)	21.4	-44.4
61	22	64.38860	3078.2 (64.2)	21.5	-42.5
42	13	65.30183	3313.1 (58.8)	21.9	-36.6
42	96	66.14591	3575.3 (164.2)	22.3	-31.2
61	25	66.45515	3275.1 (56.5)	22.6	-29.4
42	106	67.09902	2830.4 (114.8)	23.1	-25.5
61	94	67.51673	2454.9 (57.6)	23.5	-23.2
12	15	67.76315	3167.5 (184.1)	23.8	-21.8
42	114	68.10567	4054.6 (359.1)	24.1	-20.0
12	15	68.84538	5043.1 (44.4)	25.1	-16.3
42	112	69.09818	4274.0 (426.4)	25.4	-15.0
61	92	69.52428	2529.6 (340.9)	26.0	-13.1
12	19	69.78770	2308.3 (87.7)	26.3	-11.9
42	114	70.09811	2357.8 (81.0)	26.8	-10.5
61	45	70.41724	2502.6 (116.8)	27.3	-9.2
42	106	71.09232	2467.1 (39.2)	28.3	-6.5
61	86	71.54343	2298.1 (48.3)	29.1	-4.8
12	11	71.83809	2670.5 (39.2)	29.5	-3.7
61	45	72.39846	1950.5 (58.0)	30.5	-1.8
42	105	73.09167	1920.6 (56.2)	31.8	0.4
61	70	73.48775	1811.7 (43.8)	32.5	1.6

3. Coronal electron density models

3.1. Radial variation

It will be assumed that the radial and latitudinal variations of the interplanetary electron density near 0.1 AU are uncorrelated over the range of solar offset distances appropriate to the observations (21-32 $R_\odot$). The electron density at radial distance r and heliolatitude θ is thus given by:

$$N(r,\theta) = N_0 \left[\frac{R_\odot}{r}\right]^{2+\gamma} F(\theta) \tag{3}$$

where N_0 and γ are empirical parameters to be determined from the data, and

$$F(\theta) = \begin{cases} 1 & \text{for } \theta = \pm 90^\circ \\ A & \text{for } \theta = 0^\circ \end{cases} \tag{4}$$

The model parameter A in Eq. (4), to be determined from the data, is the equator-to-pole density ratio. A density model without heliolatitude dependence was derived from SCE ranging data recorded during the Ulysses in-ecliptic solar conjunction C_1 (Bird et al. 1994). Combining both ingress and egress data, the mean values of the radial parameters were $\gamma \simeq 0.48$; $N_0 \sim 2.94 \times 10^6$ cm^{-3}. The greater than inverse-square falloff in density with radius implied that the low-latitude solar wind near solar maximum was still accelerating out to a distance of 40 $R_\odot$.

Solar wind measurements recorded during the Ulysses pole-to-pole flight (Phillips et al. 1995) showed that the electron density over the poles, normalized to 1 AU, was remarkably constant: N(1 AU, $\pm 90^\circ$) $\simeq 3$ cm^{-3}. Applying this constraint to Eq. (3), one may use the resulting relation between N_0 and γ to simplify the model to a single radial parameter. Parametric values of γ were confined to the range $0.0 < \gamma < 0.5$ for this work.

3.2. Heliographic latitude variation

Various heuristic approaches have led to "traditional" models of the heliographic latitude dependence of the plasma density in the outer solar corona and inner heliosphere for solar minimum conditions. The models are characterized by a slowly varying dependence on heliographic latitude, usually invoking combinations of sine and/or cosine functions. In effect, these models are approximations that retain the lower-order terms of a more generalized expansion in Legendre polynomials (Altschuler & Perry 1972).

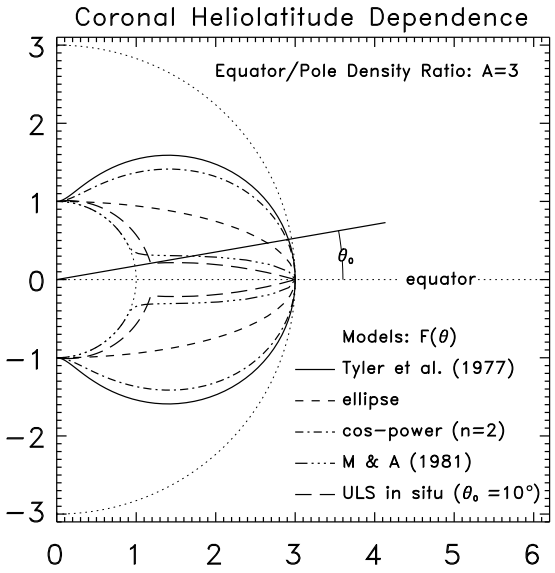

Fig. 2. Models of heliographic latitude dependence of coronal electron density $F(\theta)$. The relative increase in electron density from pole to equator is $A = 3$, and the characteristic half-width of the high-density equatorial band is $\theta_0 = 10^\circ$ for this comparison. The models are rotationally symmetric about the left vertical axis and mirror symmetric about the equator.

As an example, the model used by to simulate Viking electron content data taken during the 1976 solar occultation (Tyler et al. 1977) was given by:

$$F_1(\theta) = \sqrt{A^2 \cos^2\theta + \sin^2\theta} \tag{5}$$

with a best fit to the data using A = 8. Another possible representation would be a spheroidal distribution in latitude, for which $F(\theta)$ is a simple ellipse:

$$F_2(\theta) = \frac{A}{\sqrt{\cos^2\theta + A^2 \sin^2\theta}} \tag{6}$$

A generalized representation can also be achieved with a cosine-power law:

$$F_3(\theta) = 1 + [A - 1]\cos^n\theta \tag{7}$$

If n = 2, it can be shown that Eq. (7) reduces to the P_2 term of the Legendre series (e.g., Weisberg et al. 1976). This form for the latitudinal dependence was used by Munro & Jackson (1977) for the electron density within the confines of a polar coronal hole

These models, as plausible as they may have seemed in past years, can now be improved in the light of the new measurements on board Ulysses (Phillips et al. 1995), which effectively demonstrated the bimodel nature of the solar wind. Polar coronal holes, which map to most of the heliosphere because of their rapid expansion, produce a fast solar wind with remarkably constant velocity and density over their entire latitudinal extent. The slow solar wind, on the other hand, flows more erratically at lower velocities and higher densities in a narrow band of latitudes ($\pm 20^\circ$) roughly centered on the heliographic equator.

It is appropriate to adopt these Ulysses *in situ* results as a basis for modeling the SCE remote sensing observations much closer to the Sun. The empirically based functional form used for this approach is:

$$F_{ULS}(\theta) = \begin{cases} A - s_1 \mid \theta \mid & \text{if } \mid \theta \mid \leqq \theta_0 \\ 1.2 - s_2 \left[\mid \theta \mid - \theta_0 \right] & \text{if } \mid \theta \mid \geqq \theta_0 \end{cases} \tag{8}$$

with

$$s_1 = [A - 1.2]/\theta_0, \quad \text{and} \quad s_2 = 0.2/[90 - \theta_0]$$

where θ_0, which describes the "half-width" of the equatorial high density band, is a model parameter to be determined from the data. The density model of Eq. (8) accounts for a small (20%) increase in density from the center of the coronal hole at $\theta = \pm 90^\circ$ to the edge of the equatorial band at $\theta = \pm\theta_0$. This increase is consistent with the Ulysses *in situ* observations (Phillips et al. 1995), but does not play a major role in the model calculations to be presented in the following.

For ranging measurements close to the Sun, Muhleman & Anderson (1981) found better agreement with the 1976 Viking data using an exponential decrease in density with heliolatitude. The characteristic half-width of the higher density low-latitude band was determined to be $\theta_0 \simeq 8^\circ$. Modifying their model to retain a nonvanishing electron density at the pole, the form of this functional dependence would be:

$$F_{MA}(\theta) = 1 + [A - 1]\exp\left[-\left(\theta/\theta_0\right)^2\right] \tag{9}$$

Guhathakurta et al. (1996) have recently utilized the functional form given in Eq. (9) for a model of the electron density based on white-light observations from the photosphere out to 5 $R_\odot$. They find that the half-width of the high density band about the magnetic equator first decreases with increasing solar distance but then seems to reach a rather constant value of $\theta_0 \simeq 10^\circ$ over the range 3–5 $R_\odot$. The equator-to-pole density ratio at a solar distance of 5 $R_\odot$ derived from the same analysis was $A = 6.6$.

Figure 2 is a polar plot illustrating the heliographic latitude dependence for the coronal electron density models described by Eqs. (5–9). Traditional models such as those represented by Eqs. (5–7) feature a rather slowly varying heliolatitude dependence that contrasts with the more steeply peaked distribution of Eq. (8) observed on Ulysses. The model of Muhleman & Anderson (1981), adapted for this application with slight modifications as Eq. (9) and labeled "M & A (1981)" in Fig. 2, is a reasonable alternative to the Ulysses *in situ* model.

4. Comparison of electron content observations with model predictions

4.1. Models ordered about an equatorial symmetry plane

Calculations of total electron content during C_4 using five different models are compared with the SCE dual-frequency ranging

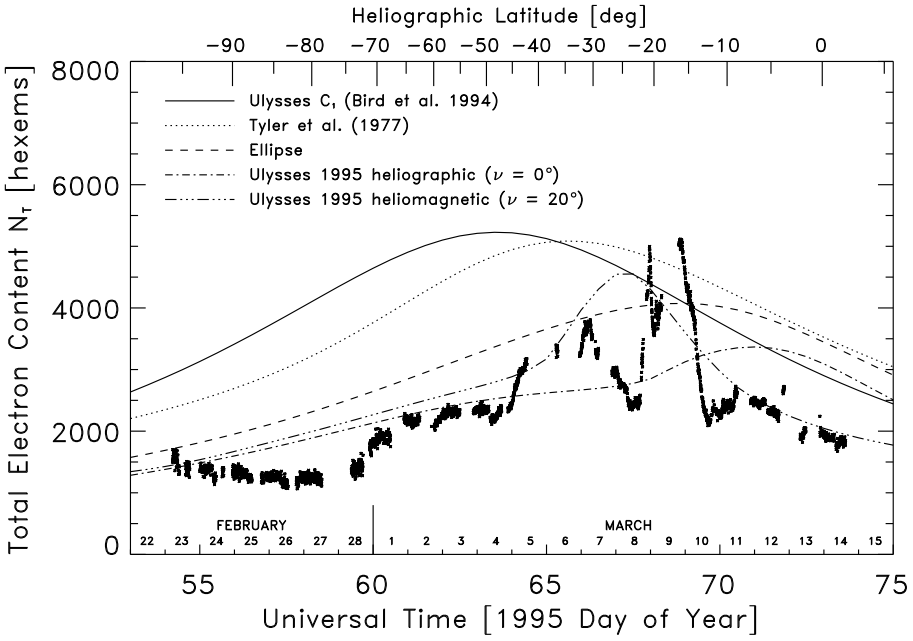

Fig. 3. Radio sounding measurements of columnar electron density during C_4 compared with simulations using five different models of coronal electron density. Heliographic latitude of the solar proximate point is plotted on the upper abscissa scale. The only model which appears to be capable of simulating the SCE column densities is the one based on Ulysses 1995 *in situ* observations, ordered about the heliomagnetic, rather than the heliographic, equator. The specific parameter set used for this example is (γ = 0.2, A = 3, θ_0 = 20°).

measurements in Fig. 3. Each individual 5-minute range measurement (total: 2829 points) is indicated by a filled square. The occasional data gaps are due primarily to incomplete tracking coverage on the heavily loaded DSN. Less than 2% of the time scheduled for SCE was lost because of equipment failures or operational errors at the ground stations.

Not unexpectedly, the spherically symmetric model from Eq. (3) with F = 1, based on Ulysses ranging data during C_1 (Bird et al. 1994: solid line), is inappropriate for the latitude scan recorded during C_4. The models of Tyler et al. (1977) from Eq. (5) or the ellipse cross-section model from Eq. (6) with γ = 0.2 and A = 3, given by the dotted and dashed lines, respectively, also yield poor representations of the SCE data. Improvements are obtained with models based on the Ulysses *in situ* data from Eq. (8), shown as the remaining curves in Fig. 3 for the parameter set (γ = 0.2, A = 3, θ_0 = 20°). The only difference between these latter two models is the choice of the equatorial symmetry plane. The model with the obviously poorer fit to the data (dash-dotted line) used the true heliographic equator as its plane of symmetry. The second model (dash-triple dotted line), however, has a density distribution ordered about a symmetry plane tilted at an angle ν = 20° with respect to the heliographic equator. The pole of this tilted plane, which simulates the heliomagnetic equator to zeroth order, was inclined toward Carrington longitude 280°. This azimuth was selected in order to achieve fair qualitative agreement with the location of the HCS inferred from solar source surface maps generated from observations made at the Wilcox Solar Observatory (WSO).

4.2. Models ordered about the heliospheric current sheet

It was recognized early in this analysis that the complex temporal profile $N_T(t)$ shown in Fig. 3 cannot be simulated with an electron density distributed symmetrically about a planar surface. A more appropriate approximation for the band of enhanced electron density is an ordering about the warped HCS. It is generally agreed (e.g., Wilcox & Hundhausen 1983) that the structure of the HCS follows that of the maximum brightness contour derived from coronal white-light polarization brightness observations (i.e., the maximum in the electron density distribution). In applying Eq. (8) in this nonplanar model, the "heliolatitude" θ must be redefined as the angular distance from the HCS.

Two models for the HCS, defined here by the magnetic neutral sheet as a function of heliographic latitude and Carrington longitude, were tested: (1) taken from spherical source surface maps at 2.5 $R_\odot$ (WSO observations: J.T. Hoeksema, private communication), and (2) derived from magnetic field reversals observed on board Ulysses (Fig. 2 in Smith et al. 1995). The relationships between the radio ray paths from Ulysses to Earth and these two heliospheric current sheets, projected onto the solar source surface at 2.5 $R_\odot$, are shown in Fig. 4.

The solar offset point (Θ, Φ) along each ray path is indicated in Fig. 4 (lower panel) by the solid dot for 1995 DOY 54–74 at 0 UT. The ray path segment yielding the middle 50% of the total columnar density $N_T(t)$ has been drawn as a solid line for DOY 60–74. To provide a qualitative indicator of the relative weights from day to day, the thickness of the ray path is scaled in linear proportion to N_T. The projection of the surface of peak electron density is given by the thick solid line for the model derived from WSO observations (HCS1), and by the thick dash-dotted line for the model derived from the Ulysses *in situ* magnetic field observations (HCS2). The strong dependence of the electron density on solar distance causes the solar proximate point to be situated near the middle of the respective mid-50% ray path segments shown in Fig. 4. The influence of the HCS, however, can induce a significant asymmetry in the locus of the mid-50% ray path about (Θ, Φ). The most obvious examples

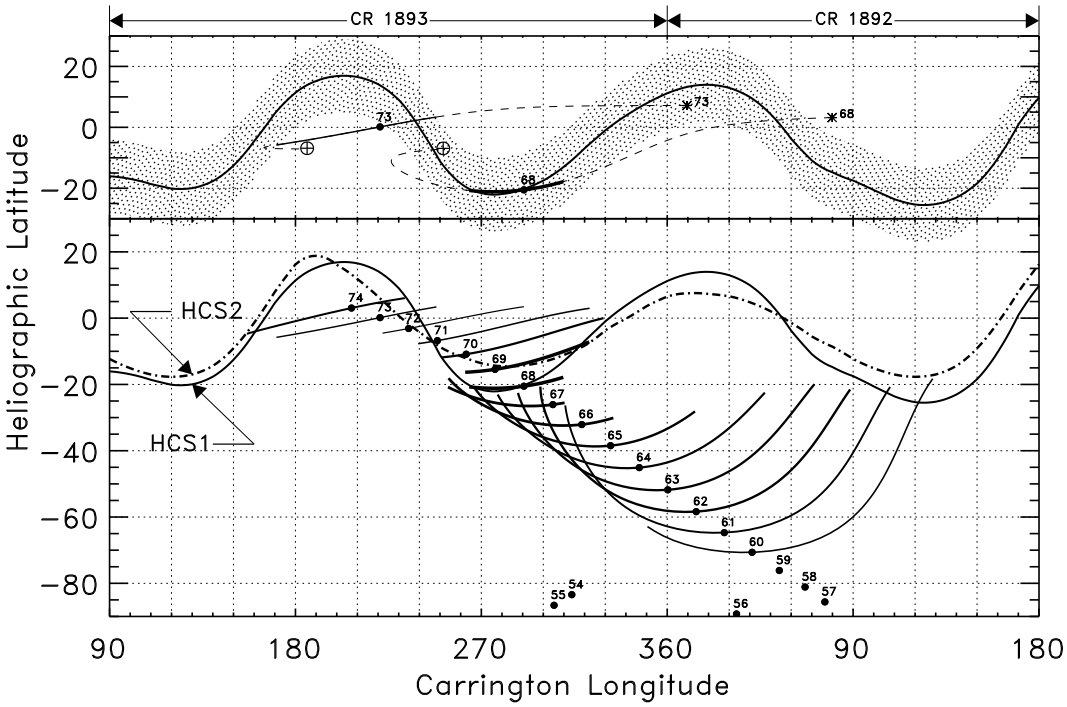

Fig. 4. Radio ray paths from Ulysses to Earth projected onto a spherical source surface at 2.5 $R_\odot$. Parts of Carrington rotations 1892 and 1893 are used for continuity of the representation. The thick solid line meandering about the heliographic equator is the trace of the heliospheric current sheet (HCS1), as inferred from potential field calculations using synoptic observations from the Wilcox Solar Observatory (kindly provided by J.T. Hoeksema, Stanford University). Lower panel: The solar proximate point along the ray path is shown as a solid dot for each 1995 DOY (0 UT) during C_4. Starting with DOY 60, the projection of the ray path segment which delivers the middle 50% of the observed total columnar density N_T has been drawn as a solid line. The thickness of the line is proportional to N_T. The thick dash-dotted line (HCS2) is the projection of the heliospheric current sheet derived from magnetic field reversals observed on board Ulysses (Smith et al. 1995). The maximum in N_T on DOYs 68–69 is clearly due to the alignment of the ray path with the HCS. Upper panel: Same as below except that now the complete ray paths are plotted for DOY 68 and DOY 73 from Ulysses (symbol: $*$) to Earth (symbol: $\oplus$). The thickness of the low-latitude high density band ($\pm 12^\circ$) is indicated by the mottled region about the HCS. The solar wind speed used to compute the co-rotation time delays for this map was taken to be v_0 = 100 km s^{-1} at 20 $R_\odot$ and v_∞ = 400 km s^{-1} (asymptotic).

of this effect are on those days when the ray paths cross the HCS near their proximate points. The electron content attained its absolute maximum during C_4 on DOYs 68–69 when the ray path was closely aligned with the HCS.

Projections of the complete ray paths on DOYs 68 and 73 are shown as examples in the upper panel of Fig. 4. The mottled region about the HCS ($\pm 12^\circ$) represents the low-latitude streamer belt with enhanced electron density. The shift in Carrington longitude $\Delta\phi$ for the projection from an arbitrary point at solar distance r was calculated from

$$\Delta\phi = \Omega_\odot \Delta t \ , \qquad \Delta t = \frac{r - 2.5 R_\odot}{v} \tag{10}$$

where $\Omega_\odot$ is the synodic solar rotation rate (13.22° day^{-1}) and v is the solar wind speed. The co-rotation time delays at the ends of the ray path (Ulysses $*$; Earth: $\oplus$), being distinctly greater than at the proximate point (solid dot), are responsible for the curious ray path distortions.

The solar wind speed was assumed to follow a radial profile given by (e.g., Beard 1979):

$$v(r) = v_\infty \exp\left[-\frac{R_H}{r}\right] \tag{11}$$

where the quantity R_H is defined by:

$$R_H = -R_0 \ln \frac{v_0}{v_\infty} \tag{12}$$

and (v_∞, v_0) are the solar wind speeds at large distance (asymptotic value) and at R_0 = 20 $R_\odot$, respectively. The particular parameters selected for the ray paths plotted in Fig. 4 were v_∞ = 400 km s^{-1}, v_0 = 100 km s^{-1}.

The density model of Eq. (3) with a latitudinal dependence given by Eq. (8) was adopted for numerical calculations of N_T from Eq. (2) for comparison with the SCE observations. The deviation of the radial falloff exponent from an inverse square dependence, denoted by the parameter γ, was found to fit the data over the southern polar regions optimally with γ = 0.0. Larger values of γ merely raised the complete profile $N_T(t)$,

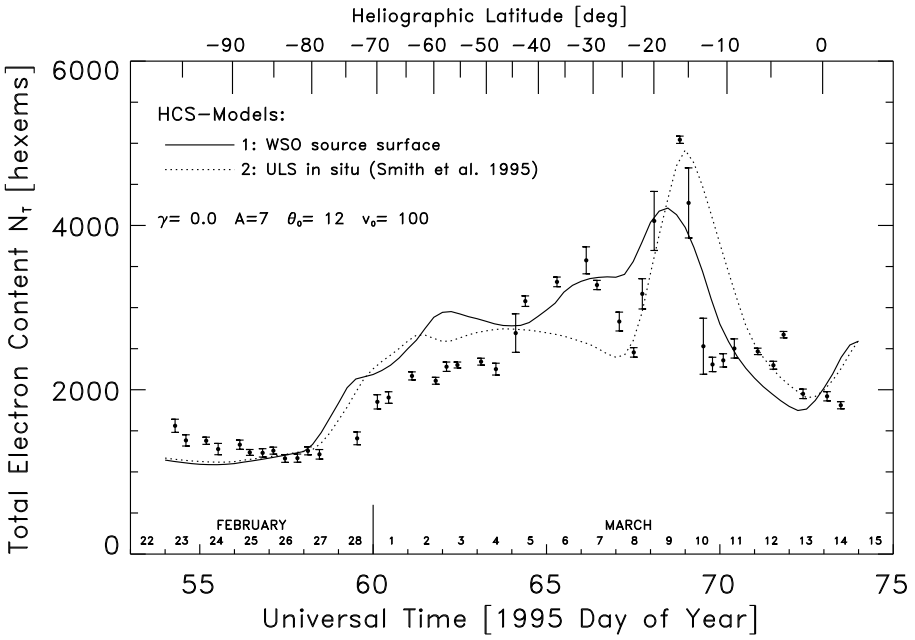

Fig. 5. Comparison of model calculations from "best" coronal density models with SCE measurements. One point (error bar: $\pm\sigma$) is plotted for each of the 42 DSN tracking passes with usable SCE data (see Table 1). The model parameters are given in the figure for the HCS locations derived from 1: WSO source surface configuration, and 2: Ulysses *in situ* observations of Smith et al. (1995). The "heliolatitude" for these models is the angular distance from the HCS. The model calculations are in rough agreement with the observations, but much of the observed fine structure cannot be simulated by either model.

the increase being slightly larger for the observations nearer the Sun. The polar electron content computed for $\gamma \geq 0.2$ was found to be too large and thus inconsistent with the assumption that $N(1\text{ AU}, \pm 90°) \simeq 3\text{ cm}^{-3}$. In view of this noncritical behavior on solar latitude, it was decided to narrow the survey down to models with only a constant value of $\gamma = 0$.

The latitudinal model parameters A and θ_0, but also the form of the solar wind speed given by Eq. (11), are responsible for producing the structure in the simulated time profile for N_T. The level of the HCS contribution to N_T was found to be roughly proportional to the product $A \times \theta_0$, the variations becoming more abrupt for heliospheric current sheets that are thinner (smaller θ_0) and denser (larger A). Within limitations, the calculated structure of $N_T(t)$ could be shifted in Carrington longitude by varying the solar wind speed. It was determined that low values of v_0 near 100–150 km s^{-1}, which are appropriate for the radial expansion of the high density regions at low latitudes, agreed much better with the observations than higher values ($v_0 > 400$ km s^{-1}). Model calculations that provide satisfactory representations of the observations are shown in Fig. 5.

For clarity, the observations displayed in Fig. 5 have been simplified to the data set given in Table 1 (i.e., one point per tracking pass, with standard deviation). The models are computed for HCS1 and HCS2 from Fig. 4, but the model parameter set is identical for the both models ($\gamma = 0$; $A = 7$; $\theta_0 = 12°$; $v_0 = 100$ km s^{-1}). Although the most salient feature of the observations, the maximum in N_T on DOYs 68–69, is reflected in the models, the peak from HCS1 comes in about a half-day too early and that from HCS2 about a half-day too late. The earlier peak from HCS1 occurs because it extends to a greater southern latitude than HCS2, thereby precipitating an earlier encounter with the upward moving Ulysses ray path.

A systematic search for the "optimum" latitudinal model parameters A and θ_0 was conducted by comparing the computed electron content predictions for each model during C_4 with the SCE observations. The parameters used in Fig. 5 were found to provide the best amplitudes and widths of the observed peaks in N_T and are surely representative of the HCS structure near 0.1 AU. Model calculations with slight differences in A or θ_0 of $\pm 10\%$ also provide satisfactory agreement. The values for the equator-to-pole density ratio $A = 7 \pm 2$ and the half-width of the equatorial high density band $\theta_0 = 12 \pm 2°$ may be compared with those inferred from solar wind measurements on board Ulysses, located at a heliocentric distance of 1.4 AU on the opposite side of the Sun from the Earth.

Beginning in February 1995, Ulysses flew several times through the HCS at essentially the same heliolongitudes probed by the spacecraft's radio link to Earth. Clear signatures of the equatorial high density sheet can be seen, for example, in the respective Figs. 1 of Phillips et al. (1995) or Gosling et al. (1995). These two figures were used to derive rough estimates of A and θ_0 for the first three crossings of the HCS recorded by Smith et al. (1995), for which complete traversals (rather than only partial penetration) of the high density band was achieved.

Assuming that the shape of the HCS in interplanetary space is a warped spiral that is convected over the Ulysses spacecraft by the radially outward flowing solar wind, the thickness of the high density band about the HCS can be derived simply from the time interval in the high density flow. It should be noted that the spacecraft does not pass perpendicularly through the high density equatorial band, thereby extending the apparent time in the region. One must account for both the tilt of the HCS and the interplanetary spiral angle in this calculation. The traversal times of 4-6 days, combined with the known, relatively slow, solar wind speeds near the HCS, yield half-widths $\theta_0 \simeq 13$–$17°$. The peak electron densities normalized to 1 AU, averaged

over six hour intervals (Phillips et al. 1995), were found to be N_e = 17, 11 and 14 cm^{-3}, respectively, for the three HCS crossings. Recalling the previously mentioned constant value of N_e = 3 cm^{-3} for the electron density at the pole, this yields typical values of $A \simeq$ 4-6. Taken at face value together with the lower corona results of A = 6.6, θ_0 = 10° (Guhathakurta et al. 1996) mentioned earlier, this would imply that the equator-to-pole density ratio A *slightly decreases* and the half-width of the equatorial density band about the HCS θ_0 *slightly increases* as the HCS structure is convected out to Ulysses at 1.4 AU.

5. Conclusions

Radio sounding of the solar corona was performed during the unique 1995 conjunction of the Ulysses spacecraft. Dual-frequency ranging observations were used to derive the columnar electron density of the inner heliosphere from pole to equator at a roughly constant solar offset distance near ∼0.1 AU. The distinct signature of the heliospheric current sheet was the most prominent feature of the latitudinal scan.

Density models of the solar corona during solar minimum that invoke slowly-varying functions of heliolatitude were determined to provide rather poor representations of the electron content observations. A better model, based on Ulysses *in situ* observations from pole-to-pole at much greater distances from the Sun, features (a) a low-density region of large solid angle, centered at the pole with very little if any, latitudinal variation, and (b) a high-density band at lower latitudes, roughly centered on the heliospheric current sheet.

For the best models, the equator-to-pole density ratio ($A \simeq 7\pm2$) was found to be marginally higher than observed by Ulysses at distances near 1.4 AU ($A \simeq$ 4-6). The characteristic half-widths of the low-latitude density band at 0.1 AU were found to be $\theta_0 \simeq 12\pm2°$, i.e., somewhat narrower than the apparent half-widths on board Ulysses ($\theta_0 \simeq$ 13–17°).

The Ulysses spacecraft has now completed its second pass over the solar poles and, with its present revolution period of 6.2 years, will return with nearly perfect timing for an additional two passes at solar maximum in the years 2000–2001. Running the Ulysses orbit into the future, it may be determined that solar conjunctions will continue to occur near spacecraft aphelion (5.4 AU). These occultations will resemble those of spacecraft in the ecliptic, however, because of the radio source's small proper motion. Moreover, power will not be sufficient for dual-frequency transmission even if Ulysses is still operational. The next occurrence of a conjunction geometry similar to C_4, as dictated by the phasing of the Earth's and Ulysses' orbits, will be in March 2026, probably too late for a repeat performance of SCE. By then, hopefully, one of Ulysses' descendants will have explored first hand those regions of circumsolar space presently accessible only to remote sensing or radio sounding.

Acknowledgements. This experiment could not have been performed without the support of the Ulysses project office, the Deep Space Network and the Multi Mission Radio Science Support Team. It is a pleasure to thank N. Angold, J. Caetta, D. Chong, P. Eshe, R. García Pérez, R. Herrera, T. Horton, A. Knight, D. Meyer, and T. Priest, all at the Jet Propulsion Laboratory. J.T. Hoeksema, Stanford University, provided the source surface map of the coronal magnetic field from the Wilcox Solar Observatory. The coronagraph image in Fig. 1 was provided by the High Altitude Observatory, National Center for Atmospheric Research (NCAR), Boulder, Colorado, USA. NCAR is sponsored by the National Science Foundation. This work was supported in part by the Deutsche Agentur für Raumfahrtangelegenheiten (DARA) under grants 50 ON 9104 and 50 ON 9401. Portions of this paper represent work done at the Jet Propulsion Laboratory, California Institute of Technology, under contract with the National Aeronautics and Space Administration. The responsibility for the contents of this publication is assumed by the authors.

References

Altschuler M.D., Perry R.M., 1972, Solar Phys. 23, 410
Anderson J.D., Krisher T.P., Borutzki M.J., et al., 1987, ApJ 323, L141
Beard D.B., 1979, ApJ 234, 696
Bird M.K., Asmar S.W., Brenkle J.P., Edenhofer P., Pätzold M., Volland H., 1992, A&AS 92, 425
Bird M.K., Asmar S.W., Edenhofer P., Funke O., Pätzold M., Volland H., 1993, Planet. Space Sci. 41, 999
Bird M.K., Edenhofer P., 1990, Remote sensing observations of the solar corona. In: Schwenn R., Marsch E. (eds.) Physics of the Inner Heliosphere. Springer, Heidelberg, p. 13
Bird M.K., Volland H., Pätzold M., Edenhofer P., Asmar S.W., Brenkle J.P., 1994, ApJ 426, 373
Coles W.A., Grall R.R., Klinglesmith M.T., Bourgois G., 1995, J. Geophys. Res. 100, 17069
Gosling J.T., Bame S.J., Feldman W.C., McComas D.J., Phillips J.L., Goldstein B., Neugebauer, M., Burkepile J., Hundhausen A.J., Acton L., 1995, Geophys. Res. Lett. 22, 3329
Guhathakurta M., Holzer T.E., and MacQueen R.M., 1996, ApJ 458, 817
Kojima M., Kakinuma T., 1992, J. Geophys. Res. 92, 7269
Manoharan P.K., 1993, Solar Phys. 148, 153
Muhleman D.O., Anderson J.D., 1981, ApJ 247, 1093
Munro R.H., Jackson B.V., 1977, ApJ 213, 874
Pätzold M., Bird M.K., Edenhofer P., Asmar S.W., McElrath T.P., 1995, Geophys. Res. Lett. 22, 3313
Pätzold M., Karl J., Bird M.K., 1996, A&A, in press
Phillips J.L., Bame S.J., Barnes A., Barraclough B.L., Feldman W.C., Goldstein B.E., Gosling J.T., Hoogeveen G.W., McComas D.J., Neugebauer M., Suess S.T., 1995, Geophys. Res. Lett. 22, 3301
Rickett B.J., Coles W.A., 1991, J. Geophys. Res. 96, 1717
Smith E.J., Balogh A., Burton, M.E., Erdös, G., Forsyth R.J., 1995, Geophys. Res. Lett. 22, 3325
Tyler G.L., Brenkle J.P., Komarek T.A., Zygielbaum A.I., 1977, J. Geophys. Res. 82, 4335
Weisberg J.M., Rankin J.M., Payne R.R., Counselman III C.C., 1976, ApJ 209, 252
Wilcox J.M., Hundhausen A.J., 1983, J. Geophys. Res. 88, 8095
Woo, R., 1996, ApJ 458, L87
Woo R., Armstrong J.W., Bird M.K., Pätzold M., 1995, Geophys. Res. Lett. 22, 329